Impurity transport in ITER-like plasmas

T. Fülöp and J. Weiland
Department of Radio and Space Science, Chalmers University of Technology and Euratom-VR Association, Göteborg, Sweden

(Received 11 August 2006; accepted 4 October 2006; published online 15 November 2006)

Neoclassical impurity transport is compared with transport calculated from the reactive drift wave model of turbulent transport for an ITER-like [R. Aymar, P. Barabaschi, and Y. Shimomura, Plasma Phys. Controlled Fusion **44**, 519 (2002)] scenario. The turbulent transport is inward for both main ions and impurities, but the impurity ion inward transport is much weaker than the main ion inward transport. The neoclassical impurity transport is outward because of temperature screening. The total impurity transport, determined by a balance between turbulent and neoclassical transport, depends sensitively on the charge number of the impurity and the ratio of the ion density and temperature scale lengths, η_i. © *2006 American Institute of Physics*. [DOI: 10.1063/1.2375042]

I. INTRODUCTION

The presence of impurities in the edge region of tokamaks can be beneficial because a strongly radiating boundary distributes plasma power loss. But many tokamak discharges suffer from unwanted and uncontrollable impurity accumulation in the plasma core and this may lead to core radiation, flat radial distribution of temperature, fuel dilution, and sometimes even disruptions. Impurity transport is critical for ITER and the issue of what governs the impurity transport should be given careful consideration.

Neoclassical transport is driven by parallel friction dynamics and is not affected significantly by the fact that the ion cross-field transport is dominated by fluctuations. Thus it is clear that neoclassical and anomalous transport coexist. The assumption that the total impurity transport is a linear sum of turbulence-driven transport and neoclassical transport has been confirmed experimentally. Reference 1 describes low-Z impurity transport in DIII-D,[2] and shows that both types of transport have to be included to explain the observed transport phenomena.

Turbulent transport of ions and impurities is usually much stronger than neoclassical theory predicts. However, it has been found in many tokamak experiments that in advanced scenarios impurity fluxes in the core may be of the order of the predictions of neoclassical theory. Reference 3 investigated the dependence of core plasma impurity transport on the charge number for ASDEX Upgrade[4] H-mode discharges and found that the impurity transport is close to neoclassical predictions for low-Z impurities, when effects related to toroidal rotation can be neglected. In Ref. 5 the impurity behavior in advanced scenarios at ASDEX Upgrade and Joint European Torus (JET)[6] was shown to be consistent with the predictions of neoclassical theory and the accumulation of impurities was connected to the main ion density peaking. In Ref. 7 the transport of impurities was measured in DIII-D in VH-mode discharges having reduced anomalous transport, and it was shown that temperature screening leads to strong outward convection of low-Z impurities. Thus, there is a strong motivation to compare neoclassical and turbulent impurity fluxes to determine which mechanism is stronger in ITER-like experimental situations.

In this work we compute the impurity transport from neoclassical theory and compare it with transport calculated from the reactive drift wave model of turbulent transport for a specific ITER-like scenario. As we will show, the total (neoclassical + turbulent) impurity flux depends sensitively on the charge number of the impurity and the ratio of the ion density and temperature scale lengths, η_i.

The structure of the paper is as follows: In Sec. II the neoclassical impurity flux is presented, both for collisionless and collisional impurities. Section III describes the reactive drift wave model used to calculate the turbulent flux. In Sec. IV neoclassical and turbulent impurity particle fluxes are compared for an ITER-like plasma, and the dependence of the transport on Z and η_i is discussed. Finally, the results are summarized in Sec. V.

II. NEOCLASSICAL TRANSPORT

Neoclassical ion transport is dominated by collisions with impurities since ion-impurity collisions are more frequent than ion-electron collisions. From the ambipolarity condition it follows that the impurity flux is oppositely directed to the ion flux $\Gamma_i=-Z\Gamma_z$. In the absence of the thermal force this should lead to impurity accumulation ($n_z\sim n_i^Z$, where n_z and n_i are the impurity and background ion densities). The accumulation can be reduced or avoided if the coefficient in front of the thermal force is negative. The outward flow induced by the thermal force, referred to as temperature screening, normally requires that the ions are collisionless and its effectiveness depends on the impurity charge and the fraction of impurities in the plasma.

The collision frequency between the species a and b is defined as[8] $\nu_{ab}=n_b e_a^2 e_b^2 \ln\Lambda/(4\pi\epsilon_0^2 m_a^2 v_{T>} v_{Ta}^2)$, where $v_{T>}$ denotes the larger of the thermal velocities v_{Ta} and v_{Tb}, and $\ln\Lambda$ is the Coulomb logarithm. The normalized collisionality is $\nu_\star^a=\nu_a qR/v_{Ta}\epsilon^{3/2}$, where $\nu_a=\Sigma_b\nu_{ab}$ is the collision frequency, q is the safety factor, R is the major radius, and $\epsilon=r/R$ is the inverse aspect ratio. Impurity-impurity collisions are more frequent than ion-ion collisions, so that heavy impurities are usually more collisional than the ions: if T_z

$\simeq T_i, \nu_\star^z = \nu_\star^i Z^{3/2}(1+\alpha\sqrt{Z})$, with $\alpha = n_z Z^2/n_i$. In today's tokamak experiments, impurities tend to lie in the collisional regime ($\nu_\star^z \epsilon^{3/2} \gg 1$). However, for ITER-like parameters (density $n_i = 10^{20}$ m^{-3}, temperature $T_i = 10$ keV, $q=2$, $R=6$ m, $\alpha \simeq 0.7$, and $\epsilon^{3/2} \simeq 0.3$), low-$Z$ impurities are collisionless ($\nu_\star^z < 1$) up to charge number $Z=11$.

In this work we calculate the impurity transport in a plasma containing background ions (i) and electrons (e) and one species of impurity (z). The ion particle flux $\mathbf{\Gamma}_i = n_i \boldsymbol{V}_i$ is given by[9]

$$\langle \mathbf{\Gamma}_i \cdot \nabla \psi \rangle = \sum_{a=i,z;k=1,2} L_{1k}^{ia} A_k^a, \tag{1}$$

where $A_1^a = \partial \ln p_a/\partial\psi$ and $A_2^a = \partial \ln T_a/\partial\psi$ are the thermodynamic forces; n_a, p_a, and T_a are density, pressure, and temperature; $\psi = -RA_\varphi$ is the poloidal flux function, $\boldsymbol{B} = I\nabla\varphi + \nabla\varphi \times \nabla\psi$ is the magnetic field;

$$L_{jk}^{ab} = 3\langle (\nabla_\parallel B)^2 \rangle \frac{I^2 T_b}{e_a e_b B_0^4} \left(\frac{\mu_{aj}\mu_{bk}}{\mu_1} - \mu_{a,j+k-1}\delta_{ab} \right) \tag{2}$$

is the transport matrix; and $\mu_1 = \mu_{i1} + \mu_{z1}$, $B_0 = \langle B^2 \rangle^{1/2}$, and $\langle \cdots \rangle$ are the flux-surface average.

A. Banana regime

The neoclassical viscosity coefficients in the banana regime are

$$\mu_{ak} = \frac{m_a n_a B_0^2}{3\langle (\nabla_\parallel B)^2 \rangle} \frac{f_t}{f_c} \left\{ \nu_D^a \left(x_a^2 - \frac{5}{2} \right)^{k-1} \right\}, \tag{3}$$

$\nu_D^a = \Sigma_b \nu_D^{ab}$ and $\nu_D^{ab}(v) = \hat{\nu}_{ab}[\phi(x_b) - G(x_b)]/x_a^3$ is the deflection frequency, with $\phi(x)$ and $G(x)$ the error and Chandrasekhar functions; $x_a = v/v_{Ta}$ is the normalized velocity; $\hat{\nu}_{ab} = \nu_{ab} v_{T>}/v_{Ta}$ and $f_c = \frac{3}{4}\int_0^{\lambda_c} \lambda d\lambda / \langle \sqrt{1 - B\lambda/B_0} \rangle$ is the effective fraction of the circulating particles $f_t = 1 - f_c$ and $\lambda_c = B_0/B_{\max}$. The braces denote the velocity integration operator $\{F(v)\} = \frac{8}{3\sqrt{\pi}} \int_0^\infty F(x v_{Ta}) e^{-x^2} x^4 dx$. The impurity flux is given by

$$\langle \mathbf{\Gamma}_z \cdot \nabla \psi \rangle = \frac{f_t}{f_c} \frac{n_i T_i I^2 \xi_z \left\{ \tilde{\mu}_{z1} [\tilde{\mu}_{i1} (\ln p_i)' + \tilde{\mu}_{i2} (\ln T_i)'] - \dfrac{T_z \tilde{\mu}_{i1}}{T_i Z} [\tilde{\mu}_{z1} (\ln p_z)' + \tilde{\mu}_{z2} (\ln T_z)'] \right\}}{m_i Z \Omega_i^2 \tau_{ii} (\tilde{\mu}_{i1} + \xi_z \tilde{\mu}_{z1})}, \tag{4}$$

where prime denotes derivative with respect to ψ, $\tilde{\mu}_{aj} = 3\langle (\nabla_\parallel B)^2 \rangle \tau_{aa} f_c (f_t m_a n_a B_0^2)^{-1} \mu_{aj}$, $\tau_{aa} = 3\sqrt{\pi}/4\hat{\nu}_{aa}$, $\xi_z = \tau_{ii} m_z n_z (\tau_{zz} m_i n_i)^{-1}$, and $\Omega_i = eB_0/m_i$. The normalized viscosity coefficients are $\tilde{\mu}_{ij} = m_j^{ii} + m_j^{iz}\alpha$ and $\tilde{\mu}_{zj} = (m_j^{zi}/\alpha\sqrt{Z}) + m_j^{zz}$, with

$$m_1^{ab} = \sqrt{1 + x_{ab}^2} + x_{ab}^2 \ln \frac{x_{ab}}{1 + \sqrt{1 + x_{ab}^2}},$$
$$m_2^{ab} = 1/\sqrt{1 + x_{ab}^2} - \frac{5}{2} m_1^{ab}, \tag{5}$$

where $x_{ab} = v_{Tb}/v_{Ta}$. The term proportional to the ion temperature gradient in Eq. (4) leads to outward transport of impurities (temperature screening). The inward flux driven by the impurity temperature gradient can be neglected, since

$$Z \frac{1 + \tilde{\mu}_{i2}/\tilde{\mu}_{i1}}{1 + \tilde{\mu}_{z2}/\tilde{\mu}_{z1}} \frac{T_i'}{T_z'} \simeq 2ZT_i'/T_z' \gg 1 \tag{6}$$

is satisfied in the parameter region of interest. Furthermore, if $|n_i'/n_i| \gg (T_i/ZT_z)|n_z'/n_z|$, also the flux driven by the impurity density gradient can be neglected. A criterion for the outward transport of impurities can then be derived to be $n_i'(\eta_i - \eta_i^t) < 0$, where $\eta_i = (n_i T_i'/n_i' T_i) = L_{ni}/L_{Ti}$ is the ratio between the ion density and temperature scale lengths, and $\eta_i^t \equiv -\tilde{\mu}_{i1}/(\tilde{\mu}_{i1} + \tilde{\mu}_{i2})$.

In the cylindrical, large aspect ratio limit the impurity flux can be written in simpler form as

$$\langle \mathbf{\Gamma}_z \cdot \nabla r \rangle = \frac{f_t}{f_c} \frac{n_i T_i \xi_z m_i q^2}{e^2 Z B_0^2 \epsilon^2 \tau_{ii}} \frac{\tilde{\mu}_{z1}}{\tilde{\mu}_{i1} + \xi_z \tilde{\mu}_{z1}} \times \left[\tilde{\mu}_{i1} \frac{d \ln n_i}{dr} + (\tilde{\mu}_{i1} + \tilde{\mu}_{i2}) \frac{d \ln T_i}{dr} \right], \tag{7}$$

where we neglected the flux driven by impurity density and temperature gradients and approximated the derivative with respect to ψ as $\partial/\partial\psi \simeq 1/RB_p(\partial/\partial r)$, where B_p is the poloidal magnetic field. In this limit $B_p/B \simeq \epsilon/q$ and the effective fraction of trapped particles can be approximated as $f_t = \sqrt{2\epsilon/(1+\epsilon)}$. If the impurity-ion density ratio n_z/n_i is constant, then $\xi_z = \alpha^2 \sqrt{m_z/m_i}(T_i/T_z)^{3/2} \simeq \alpha^2\sqrt{Z}$ is strongly dependent on Z and the flux increases with Z. This behavior has been confirmed experimentally.[7] However, if $Z_{\text{eff}} \equiv (n_z Z^2 + n_i)/(n_z Z + n_i)$ is assumed to be constant, then the fraction of impurities n_z/n_i decreases with increasing Z, and $\xi_z \simeq \sqrt{Z}$. As a consequence, the neoclassical transport decreases weakly with increasing Z.

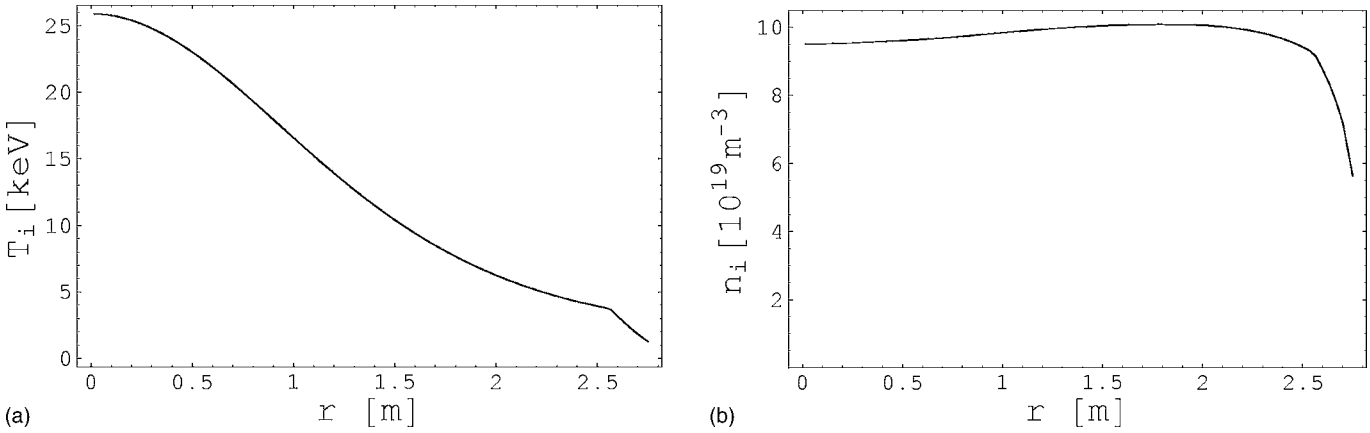

FIG. 1. Radial temperature and density profiles as a function of minor radius in the ITER high-Q scenario.

B. Mixed-collisionality regime

Even in ITER, impurities with high Z may be collisional, especially at the edge, where the temperature is low. The impurity flux is given by

$$\langle \Gamma_z^c \cdot \nabla \psi \rangle \simeq \frac{2q^2 \langle \nabla \psi \rangle^2}{m_i Z \Omega_i^2 \tau_{iz}} \left[\frac{\partial p_i}{\partial \psi} - \frac{3n_i}{2} \frac{\partial T_i}{\partial \psi} - \frac{n_i}{n_z Z} \frac{\partial p_z}{\partial \psi} \right]. \tag{8}$$

III. ANOMALOUS TRANSPORT IN THE REACTIVE DRIFT WAVE MODEL

The reactive model used here[10] (usually called Weiland model) has been used extensively in describing the present international tokamak database (JET, ASDEX, DIII-D) and also for making ITER predictions.[11] It uses an "advanced" reactive fluid model where "advanced" here refers to the rule for closure which allows us to use the model close to the fluid resonance in the collisionless case. In the version used here it has two independent ion species with the same physics included for both. The particle transport for the main species was tested successfully on JET discharges in Ref. 12. The particle pinch depends particularly strongly on the magnetic drift frequency. Because of this, species with higher Z have a weaker particle pinch thus giving a favorable net effect on the effective Z. The particle pinch is particularly relevant for ITER since central fueling will not be possible there. In fact, the particle pinch has been found to improve ITER performance significantly.

The transport coefficients used in the calculations are derived using quasilinear theory.[13–15] The saturation level can be estimated by a balance between the linear growth and the dominant $\boldsymbol{E}\times\boldsymbol{B}$ convective nonlinearity as

$$\frac{e\phi}{T_e} \simeq \frac{1}{k_x \rho_s} \frac{\gamma}{k_y c_s}, \tag{9}$$

where x and y are slab coordinates corresponding to radial and poloidal coordinates, $\boldsymbol{k}$ is the wavenumber of the unstable wave, ϕ is the electrostatic potential, $\rho_s = c_s/\Omega_i$, c_s is the sound speed, γ is the linear growth rate of the unstable mode and the components of the wavenumber are assumed to be $k_x\rho_s \simeq k_y\rho_s \simeq \sqrt{0.1}$. The impurity transport is given by

$$\Gamma_z = \delta n_z v_E^* + \text{complex conjugate}, \tag{10}$$

where $v_E = -ik_y\phi/B$ and δn_z is the impurity density perturbation due to the turbulence given by[10]

$$\frac{\delta n_z}{n_z} = \frac{L_{ne}}{L_{nz}} \frac{\omega_{\star e}}{N_z} \left[\omega(1-\epsilon_{nz}) + \left(\eta_z - \frac{7}{3} + \frac{5}{3}\epsilon_{nz} \right) \omega_{Dz} \right] \frac{e\phi}{T_e}, \tag{11}$$

where $N_z = \omega^2 - 10\omega\omega_{Dz}/3 + 5\omega_{Dz}^2/3$, $\omega_{\star a}$ is the diamagnetic frequency, ω_{Da} is the magnetic drift frequency, $\epsilon_{na} = \omega_{Da}/\omega_{\star a}$, $L_{na} = -n_a/n_a'$, and $L_{Ta} = -T_a/T_a'$ are the density and temperature scale lengths for particle species a and $\eta_z = L_{nz}/L_{Tz}$. The imaginary part of the density perturbation is given by

$$\Im\left\{ \frac{\delta n_z}{n_z} \right\} = \frac{L_{ne}}{L_{nz}} \frac{1}{\epsilon_{ne} |\bar{N}_z|^2} \left[(\bar{\gamma}\bar{N}_{zr} - \bar{\omega}_r \bar{N}_{zi})(1-\epsilon_{nz}) + \left(\eta_z - \frac{7}{3} + \frac{5}{3}\epsilon_{nz} \right) \tau_z \bar{N}_{zi} \right] \frac{e\phi}{T_e}, \tag{12}$$

where the overbar denotes normalization with respect to the electron magnetic drift frequency $\omega_{De} = 2k_y T_e/eBR$, $\tau_z = T_z/(ZT_e)$, and N_{zr} and N_{zi} are the real and imaginary parts of N_z. Using Eqs. (9) and (12) in (10), we can calculate the impurity diffusion coefficient D_z, defined by $\Gamma_z = -D_z \partial n_z/\partial r$ to be

$$D_z = 2\bar{\gamma}^3 \frac{\rho_s c_s}{R k_y} (\Delta_1 - \Delta_T \eta_z + 2\Delta_2 L_{nz}/R), \tag{13}$$

where $\Delta_T = 2\tau_z(\bar{\omega}_r + 5\tau_z/3)/|\bar{N}_z|^2$, with

$$\Delta_1 = [\bar{\omega}_r^2 + \bar{\gamma}^2 + 14\bar{\omega}_r\tau_z/3 + 55\tau_z^2/9]/|\bar{N}_z|^2,$$

$$\Delta_2 = -[\bar{\omega}_r^2 + \bar{\gamma}^2 + 10\bar{\omega}_r\tau_z/3 + 35\tau_z^2/9]/|\bar{N}_z|^2,$$

where $|\bar{N}_z|^2 = N_{zr}^2 + N_{zi}^2$, with $N_{zr} = \bar{\omega}_r^2 - \bar{\gamma}^2 + 10\tau_z\bar{\omega}_r/3 + 5\tau_z^2/3$ and $N_{zi} = 2\bar{\gamma}(\bar{\omega}_r + 5\tau_z/3)$. These expressions are in agreement with the corresponding ones given in Refs. 15 and 16.

The diffusion coefficient derived above is for the electrostatic case, but electromagnetic effects only influence the unstable wave frequency and have no effect on the expres-

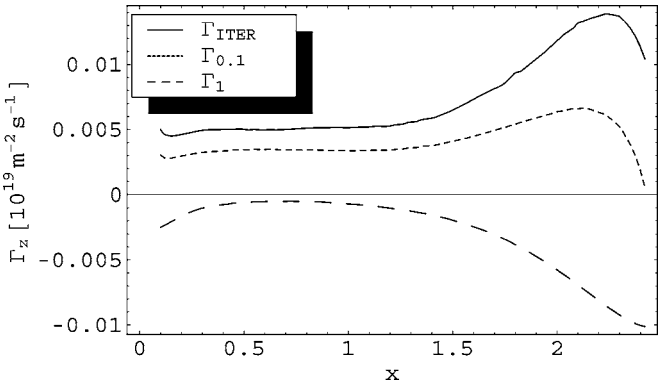

FIG. 2. Neoclassical impurity particle transport for the selected ITER scenario (solid), for a flat density profile with $n_{0.1}=n_i(0)(1-(r/a)^2)^{0.1}$ (dotted), and for a peaked density profile $n_1=n_i(0)(1-(r/a)^2)$ (dashed) as functions of radius for impurity charge $Z=10$. Note that the neoclassical transport is outward only for flat density profiles.

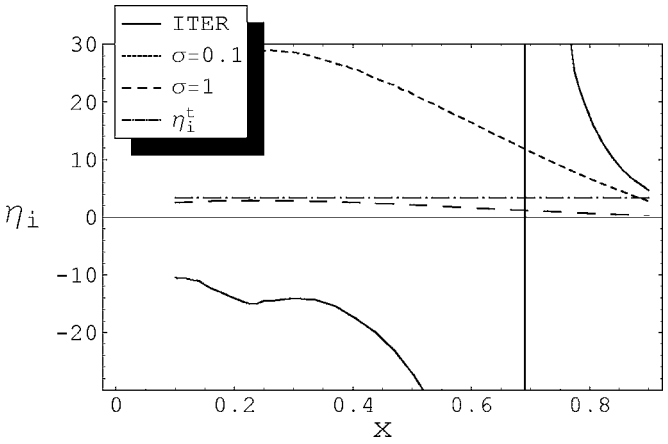

FIG. 3. η_i for the density profiles used in Fig. 2 as functions of $x=r/a$ together with the threshold for η_i, denoted by η_i^t, for $Z=10$. If $\eta_i>\eta_i^t$ or $\eta_i<0$, the neoclassical impurity transport is outward.

sion for the impurity diffusion coefficient. The frequency and growth rate of the unstable mode, $\bar{\omega}=\bar{\omega}_r+i\bar{\gamma}$, are determined numerically, including electromagnetic effects.

It is well known that the growth rate of the main ion temperature gradient (ITG) mode is reduced by dilution.[13] This would tend to reduce the turbulent particle transport. However, for sufficiently large impurity density the impurity ITG takes over. The growth rate of this mode increases with impurity density and, accordingly, also the turbulent particle transport increases. Thus, although the impurity density does not appear explicitly in our formulas, it is an important parameter. In the following section, the results of Eqs. (7), (8), and (13) will be compared with numerical calculations of the turbulent transport for ITER-like parameters and different impurity species. In these calculations we keep $Z_{\mathrm{eff}}\simeq 1.7$ constant.

IV. IMPURITY FLUX IN ITER

For a specific high-Q ITER-like scenario,[17] with minor radius $a=2.75$ m, major radius $R=6.2$ m, and magnetic field at the axis $B=5.3$ T, the radial temperature and density profiles are given in Fig. 1. For the ITER scenario we selected, the density profile is slightly hollow and is much flatter than the temperature profile. For flat density profiles, η_i is large and the neoclassical transport is outward. The reason for the outward flow is temperature screening, that is effective when $\eta_i>\eta_i^t\simeq 3.5$, if both the ion density and temperature gradients are negative. Note that even if the density gradient is locally positive $n_i'(\eta_i-\eta_i^t)<0$ is satisfied, because η_i is then negative (assuming that the temperature gradient is still negative). However, it is interesting to note that a more peaked density profile reduces the effect of temperature screening and should reduce the outward transport. In Fig. 2 the influence of the peakedness and the hollowness on the impurity transport is illustrated by modeling the main ion density by $n_\sigma=n_i(0)(1-(r/a)^2)^\sigma$ and for various σ comparing the impurity transport with the transport in the case of the density profile shown in Fig. 1. The impurity outward transport is higher for the hollow profile shown in Fig. 1 than for the flat profile with $\sigma=0.1$, especially in the outer part of the plasma. The transport changes sign if the parameter $\sigma>0.9$, since a strong density gradient overwhelms the temperature screening. Figure 3 shows η_i as a function of the normalized

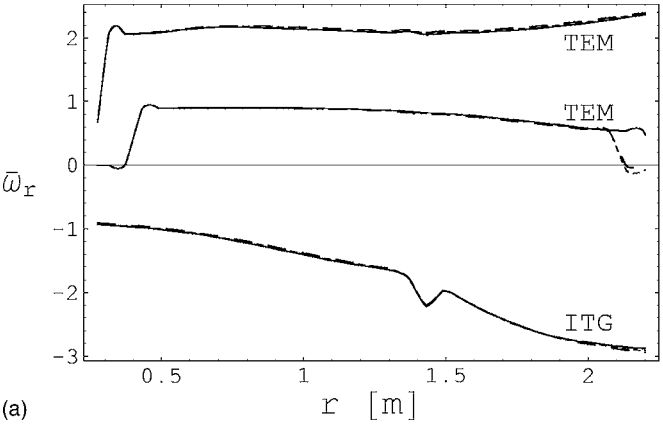

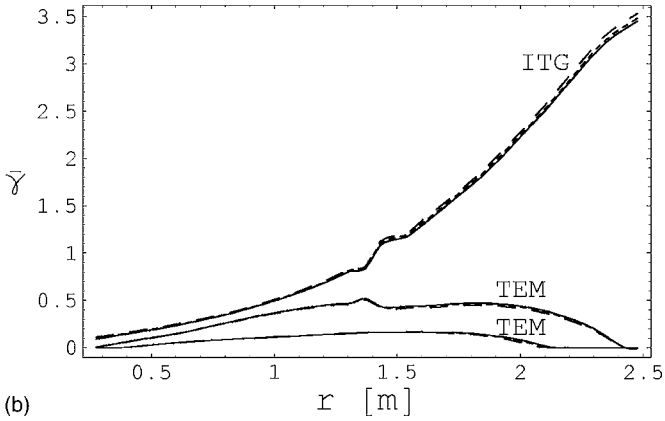

FIG. 4. The real part of the frequency $\bar{\omega}_r$ and the growth rate $\bar{\gamma}$ of the unstable ITG mode and the two most unstable TEM modes, normalized to the electron magnetic drift frequency, for $Z=6$ (solid), $Z=10$ (dotted), $Z=54$ (dashed). The curves for different impurity charges overlap, indicating that the frequency and growth rate of the unstable modes are not sensitive to Z. The ITG mode has negative real frequency and larger growth rate than the TEM modes.

radius for the various density profiles used in Fig. 2, together with the threshold for η_i, denoted by η_i^t.

The transport due to the impurity gradients is more than an order of magnitude lower than the transport due to the ion gradients for this specific ITER scenario.

Comparison of turbulent and neoclassical transport

The turbulent transport is caused by the ITG mode and trapped electron (TEM) mode. The real part of the frequency and the growth rate for the numerically calculated unstable modes are given in Fig. 4. The growth rate of the ITG mode is considerably larger than the growth rate of the TEM modes, and its real frequency is negative while the real frequencies of the TEM modes are positive. The impurity transport is inward when $\Delta_1-\Delta_T\eta_z+2\Delta_2 L_{nz}/R<0$, which is satisfied by impurities with any Z in this specific ITER-like scenario. Figure 5 shows the neoclassical and the numerically calculated turbulent impurity particle transport as a function of the normalized radius for impurity charges $Z=6$, 10, 54. It is interesting to note that neoclassical and turbulent transport have opposite signs.

The numerical calculations show that turbulent transport is dominated by the unstable ITG mode. The convective part of the transport, proportional to Δ_2, dominates, and that gives an inward flux of impurities. The terms proportional to Δ_1 and Δ_T give rise to outward transport (for the ITG mode), but they are negligible inside the radius $r/a<0.7$. Noting that for $r/a<0.7$, $\Delta_2\simeq -1/(\bar{\omega}_r^2+\bar{\gamma}^2)$, we can rewrite the convective part of the flux as

$$\Gamma_z^{\text{turb}} \simeq -\frac{2\bar{\gamma}^3}{\bar{\omega}_r^2+\bar{\gamma}^2}\frac{T_{\text{keV}}^{3/2}n_z}{B^2}, \tag{14}$$

where T_{keV} is the ion temperature in keV. The flux given in Eq. (14) is approximately equal to the total turbulent flux inside the radius $r/a<0.7$. Outside this radius, the terms proportional to Δ_1 and Δ_T become comparable to the convective part, and reduce the inward transport, so much that it sometimes even changes sign at the edge.

Assuming flat density profiles, so that the flux driven by the ion density gradient can be neglected, the neoclassical flux in the banana regime can be approximated as

$$\Gamma_z^{neo} \simeq -2\cdot 10^{16}\frac{f_t}{f_c}\frac{q^2 n_{19}^2 T'_{\text{keV}}}{ZB\epsilon^2 T_{\text{keV}}^{3/2}R} \tag{15}$$

for $r/a<0.7$, where n_{19} is the ion density in units of 10^{19} m^{-3}. Using these approximate expressions for the neoclassical and turbulent transport we can determine the charge number for which the outward neoclassical transport is larger than the inward turbulent transport,

$$Z > Z_{\text{eff}} + 10^3\frac{Z_{\text{eff}}-1}{B}\frac{\epsilon^2}{q^2}\frac{f_c}{f_t}\frac{\bar{\gamma}^3}{\bar{\omega}_r^2+\bar{\gamma}^2}\frac{T_{\text{keV}}^3 R}{T'_{\text{keV}}n_{19}}. \tag{16}$$

For low-Z impurities, the inward turbulent transport dominates. However, the main ion inward transport is at least an order of magnitude larger.

The growth rate of the unstable ITG mode increases with η_i, so that the turbulent transport (which is normally inward) increases. Even if η_i is large, leading to strong outward neoclassical transport, the resulting (turbulent + neoclassical) transport can be inward, if the turbulent transport is large enough to dominate over neoclassical transport. Figure 6 shows the total (turbulent + neoclassical) impurity transport as a function of η_i, for impurity charges $Z=6$, 10, 54. For low Z, the impurity transport depends sensitively on η_i. The direction of the impurity flux is inward if η_i is large and negative (flat and slightly hollow profiles), and the threshold is at $\eta_i\simeq -10$. Below $\eta_i\simeq -10$ turbulent transport dominates and the total impurity transport is inward. For large and positive η_i (outside $r/a=0.7$), inward transport caused by the convective term Δ_2 is counteracted by the outward transport

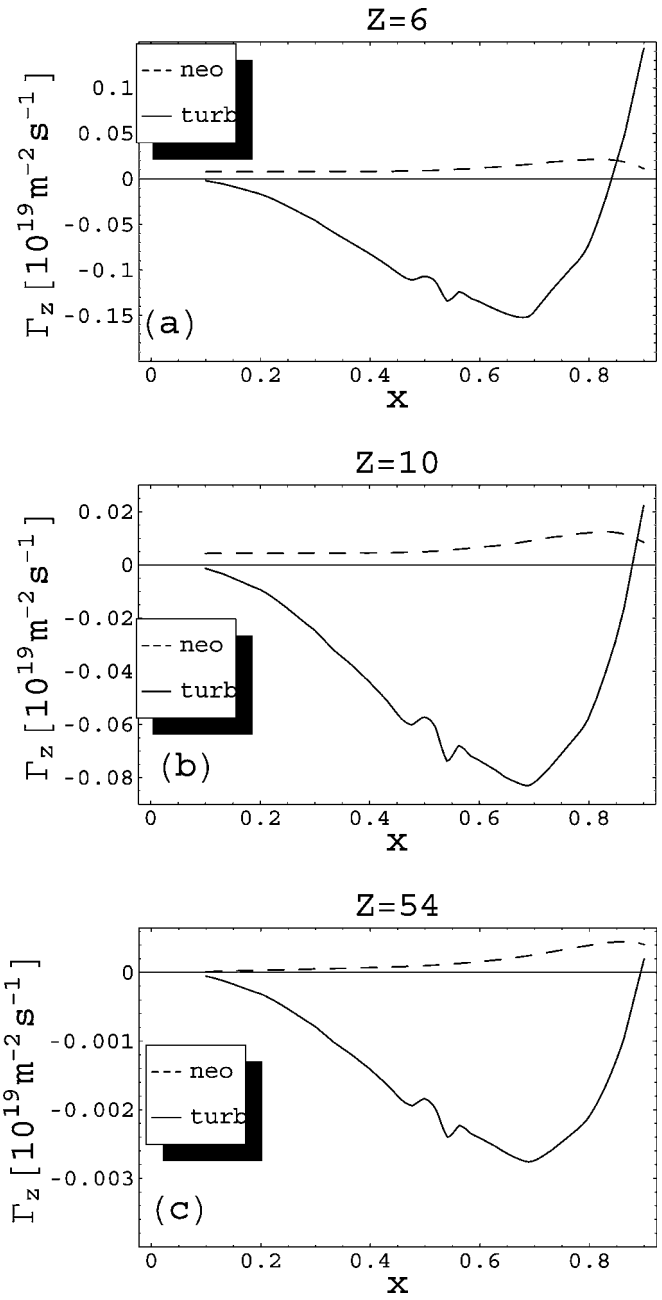

FIG. 5. Neoclassical (dashed) and turbulent (solid) impurity particle transport as a function of normalized radius $x=r/a$ for impurity charges $Z=6$, 10, 54.

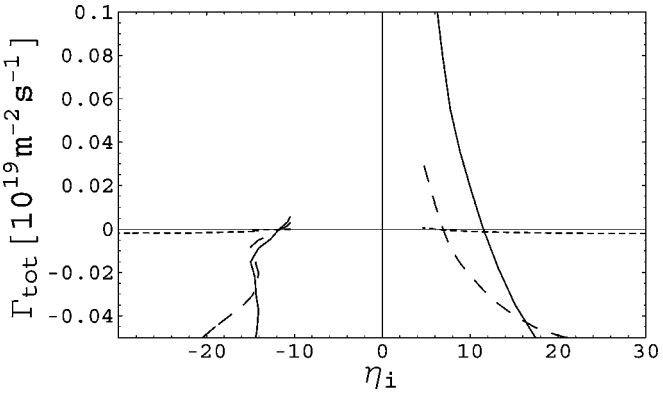

FIG. 6. Total (turbulent + neoclassical) impurity transport as a function of η_i, for $Z=6$ (solid), $Z=10$ (dashed), $Z=54$ (dotted). For large Z, the impurity transport is always inward, but weak. For low Z, the impurity transport depends sensitively on η_i.

caused by Δ_1 and Δ_T, and the neoclassical transport, so that the total transport is outward if η_i is not too large.

Our expression for the impurity diffusion coefficient (13) agrees with Eqs. (5)–(8) of Ref. 16, and it shows that the magnitude (and sometimes even the direction) of the anomalous flux depends on the sign of the real frequency of the unstable mode, which is different for the ITG and TEM modes. The TEM mode, with a positive real frequency, gives rise to an inward flux, while the ITG mode can give rise to both inward and outward flux depending on the relative magnitude of the terms Δ_1, Δ_T, and Δ_2. In our calculations for the chosen ITER profile, the ITG mode is dominant, and the anomalous flux is inward, except for low-Z impurities in the edge plasma.

Figure 7 shows the turbulent and neoclassical *ion* particle transport for $Z=6$, 10, 54. Turbulent ion particle transport is not sensitive to the charge number. Both turbulent and neoclassical ion transport are inward. Although the magnitude of the neoclassical transport is Z times larger than the impurity transport, it is still smaller in comparison with turbulent ion transport by at least a factor of 20.

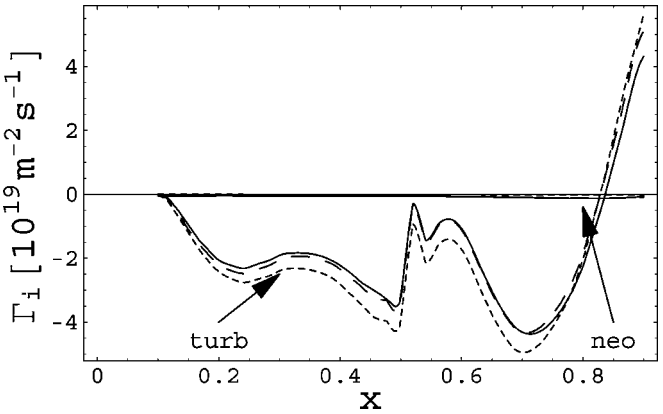

FIG. 7. Main ion turbulent and neoclassical transport as a function of normalized radius $x=r/a$, for $Z=6$ (solid), $Z=10$ (dashed), $Z=54$ (dotted). The turbulent transport is inward except for the edge plasma.

V. CONCLUSIONS

The direction of the total impurity flux depends on the impurity charge number Z and the ratio of ion density and temperature scale lengths η_i. If Z is high (collisional impurities), then impurity transport is inward for all η_i. If Z is low (collisionless impurities), then the direction of the total impurity flux depends sensitively on η_i. If $|\eta_i| \lesssim 10$ the total flux is outward, but if $|\eta_i| \gtrsim 10$, then turbulent transport dominates over neoclassical and the total transport is inward.

In this work we have only determined the direction and magnitude of the impurity flux for a given ITER scenario, at a specific time, and we did not analyze the evolution of the impurity profiles in time. If the density profile becomes more peaked as the turbulence drives the main ions inward, η_i changes, and then both the direction and magnitude of the impurity flux will change.

Our analysis assumes that the effect of the interaction between different impurity species and charge states can be neglected. This assumption is justified in case the impurity density is low, so that collisions among different species may be neglected. Furthermore, we neglect the effect of plasma rotation, since it is not expected to be very strong in ITER. However, we note that toroidal plasma rotation may enhance the neoclassical impurity transport,[18] especially for heavy impurities.

Our conclusions are in qualitative agreement with the conclusions of Ref. 19. In Ref. 19 impurity behavior was numerically calculated for ITER operational scenarios and it was shown that for flat density profiles, temperature screening prohibits impurity accumulation in the core. However, our analysis shows that, depending on the sign and magnitude of η_i, even for low Z, turbulent transport may dominate over neoclassical, and the direction of the impurity particle flux may be inward. However, the turbulent transport of main ions is usually also inward and dominates the effect on the charge balance.

ACKNOWLEDGMENT

This work was funded by the European Communities under Association Contract between EURATOM and *Vetenskapsrådet*.

[1] M. R. Wade, W. A. Houlberg, L. R. Baylor, W. P. West, and D. R. Baker, J. Nucl. Mater. **290-293**, 773 (2001).
[2] J. Luxon, Nucl. Fusion **42**, 614 (2002).
[3] R. Dux, A. G. Peeters, A. Gude, A. Kallenbach, and R. Neu, Nucl. Fusion **39**, 1509 (1999).
[4] S. Günter, C. Angioni, M. Apostoliceanu *et al.*, Nucl. Fusion **45**, S98 (2005).
[5] R. Dux, C. Giroud, R. Neu, A. G. Peeters, J. Stober, and K.-D. Zastrow, J. Nucl. Mater. **313-316**, 1150 (2003).
[6] P. H. Rebut, Nucl. Fusion **25**, 1011 (1985).
[7] M. R. Wade, W. A. Houlberg, and L. R. Baylor, Phys. Rev. Lett. **84**, 282 (2000).
[8] R. D. Hazeltine and J. D. Meiss, *Plasma Confinement* (Addison-Wesley, Redwood City, CA, 1992).
[9] P. Helander and D. J. Sigmar, *Collisional Transport in Magnetized Plasmas* (Cambridge University Press, Cambridge, 2002).
[10] J. Weiland, *Collective Modes in Inhomogeneous Plasma* (IOP, Bristol, 2000); J. Weiland, A. Jarmén, and H. Nordman, Nucl. Fusion **29**, 1810 (1989).
[11] M. Wakatani, V. S. Mukhovatov, K. H. Burrell *et al.*, Nucl. Fusion **39**,

2175 (1999); V. Mukhovatov, M. Shimada, A. N. Chudnovskiy *et al.*, Plasma Phys. Controlled Fusion **45**, A235 (2003).
[12]L. Garzotti, X. Garbet, P. Mantica *et al.*, Nucl. Fusion **43**, 1829 (2003).
[13]M. Fröjdh, M. Liljeström, and H. Nordman, Nucl. Fusion **32**, 419 (1992).
[14]G. Bateman, J. Weiland, H. Nordman, J. Kinsey, and C. Singer, Phys. Scr. **51**, 597 (1995).
[15]M. Fröjdh, P. Strand, J. Weiland, and J. Christiansen, Plasma Phys. Controlled Fusion **38**, 325 (1996).
[16]C. Angioni and A. G. Peeters, Phys. Rev. Lett. **96**, 095003 (2006).
[17]A. Polevoi (private communication).
[18]P. Helander, Phys. Plasmas **5**, 1209 (1998).
[19]V. M. Leonov and V. E. Zhogolev, Plasma Phys. Controlled Fusion **47**, 903 (2005).